Classification and Monitoring of Early Stage Breast Cancer using Ultra Wideband Radar

Marggie Jones, Dallan Byrne, Brian McGinley,
Fearghal Morgan , Martin Glavin, Edward Jones and Martin O'Halloran
College of Engineering and Informatics
National University of Ireland Galway
University Road, Galway, Ireland
Email: marggie.jones@gmail.com, dallan.byrne@gmail.com, brian.mcginley@gmail.com, fearghal.morgan@nuigalway.ie, martin.glavin@nuigalway.ie, edward.jones@nuigalway.ie, martin.ohalloran@nuigalway.ie

Raquel C. Conceição
Instituto de Biofísica e Engenharia Biomédica
Faculdade de Ciências
Universidade de Lisboa
Portugal
Email: raquelcruzconceicao@gmail.com

***Abstract*—This paper presents a novel Self-Organising Map for breast cancer classification and monitoring, based on Microwave/Ultra Wideband radar imaging. This approach has the potential to help clinicians to differentiate and track the development of a tumour from a benign state to different levels of malignancy based on their Radar Target Signature (RTS). Many existing studies have investigated the use of the RTS of a tumour to classify breast cancer as either benign or malignant, based on the fact that the RTS of a tumour is dependent on tumour shape, size and surface texture. In this paper, a self-organising (Kohonen) map is applied to the salient features of the tumour RTSs, developing a two-dimensional "MammoMap", where the various regions of the map correspond to the characteristics (benign or malignant) of the tumour, potentially allowing for the allowing for the classification and monitoring of tumour growth.**

***Keywords*-Microwave Imaging; Breast Cancer; Classification; radar**

I. INTRODUCTION

In the US, between 4%-34% of all breast cancers are missed by conventional X-Ray mammography [1], while 70% of all malignancies identified are found to be benign after biopsy [2]. These false positive conclusions result in unnecessary biopsies, causing considerable distress to the patient and an unnecessary financial burden on the health service [2], [3]. In the US, more than 184,000 new cases of breast cancer are diagnosed each year resulting in approximately 41,000 deaths. Early detection and intervention is one of the most significant factors in improving the survival rates and quality of life experienced by breast cancer patients [4], since this is the time when treatment is most effective.

Ultra Wideband (UWB) radar imaging is one of the most promising emerging breast imaging modalities. The physical basis of UWB radar imaging is the dielectric contrast between normal and malignant breast tissue that exists at microwave frequencies [5], [6], [7], [8], [9], [10]. This dielectric contrast is due to the increased water content present in the cancerous tissue, and this contrast suggests that when the breast is illuminated by a UWB pulse, cancerous tissue in the breast tissue will provide backscattered energy, which may be used to detect, localise, classify and track tumour development. UWB radar imaging is non-ionising, non-invasive, does not require uncomfortable breast compression, and is potentially low cost.

Several studies have also examined the use of UWB radar to classify breast cancer. This classification approach is based on the Radar Target Signature (RTS), which reflects the size, shape and surface texture of the tumour. Benign tumours typically have smooth surfaces and have spherical, oval or at least well-circumscribed contours. Conversely, malignant tumours usually present rough and complex surfaces with spicules or microlobules, and their shapes are typically irregular, ill-defined and asymmetric [11]. These tumour characteristics are generally reflected in the details of the RTS and can be used to differentiate between benign and malignant tumours, potentially negating the need for tumour biopsy.

In this paper, a Self-Organising Map (SOM) tumour classification and monitoring algorithm is considered. The map is described as "self-organising" since the learning process is completely unsupervised. In the implementation considered in this paper, the SOM produces a two-dimensional map, where the map is divided into a number of distinct regions. These regions can correspond to either tumour size (large or small) or tumour type (benign or malignant), depending

 ISBN: 978-1-61208-246-2

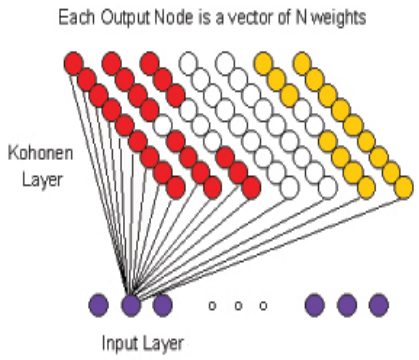

Figure 1. Kohonen SOM topology, adapted from [13]. Each output layer node is represented by an N-dimensional weights vector.

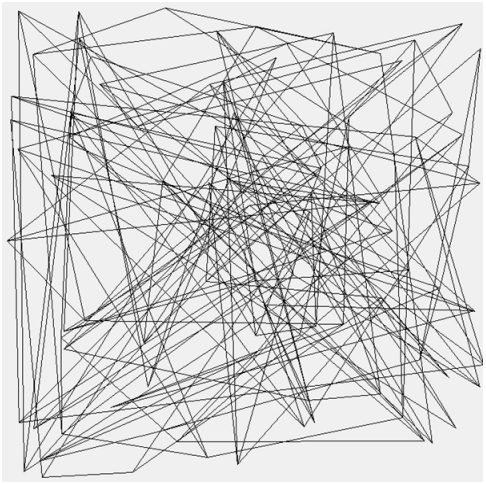

Figure 2. Plot of network weights directly after random initialization.

on the specific application. These "MammoMaps" could provide a very intuitive visual aid to clinicians for the diagnosis, monitoring and treatment of early stage breast cancer.

Self-organising maps are briefly described in the next section. This is followed by a discussion of tumour shape and electromagnetic modelling. In Section 4 details of the feature extraction method used are given. Results and discussion follow in Section 5, and finally a conclusion is drawn and future work proposed in Section 6.

II. Self-Organising Maps

Self-Organising Maps (SOMs) are a type of neural network that are trained using unsupervised learning, where the input pattern is applied and the network produces the output without being told what output should be produced [12]. Self-organising maps consist of an input and an output layer. The topology of a SOM network is shown in Figure 1. The dimension of the input layer is defined as being equal to the number of features or attributes, while the output layer is typically a two-dimensional grid (shown as red, white and yellow regions in Figure 1). In SOMs, the two layers are fully interconnected i.e., each input (ip_i) is connected to every unit or node in the output layer.

To illustrate the operation of the SOM, two-dimensional data is employed here, showing the topological mapping of the data. Although, 2-D data is used here for illustration purposes, the SOM performs very well in organising much-higher dimensional data such as that generated by the UWB feature-extraction methods used in this paper. The 2-D input data is randomly initialised and evenly distributed over the range zero to one. Weightings, wt_{j1} and wt_{j2}, initially also randomly selected from the same range, are associated with the inputs to each node j. These weights are adapted so that the network of weights, as an entirety, organises to form topological mappings of the input space. This means that the distribution of weight values in the network will reflect the distribution of input data. Details of how these network weights are adapted are given in the following section.

To more easily visualise the topological distribution of network weights, a graph is plotted with a point for each node in the output layer, the co-ordinates of each point being given by the weight values of the node (e.g. ordinate value wt_{j1} and abscissa value wt_{j2}). If nodes in the output layer are assigned indices (i, j) denoting their row and column, then joining the point for node (i, j) to the points for nodes $(i + 1, j)$ and $(i, j + 1)$ for every node in the output layer yields a plot similar to Figure 2. Figure 2 illustrates randomly selected weights chosen from the range zero to one before the Kohonen training process was applied (i.e., the plot was made directly after initializing the weight values).

A. Network Training

Having randomly initialized the weight values, the training process described by Kohonen [12] now begins. For training, the following steps are repeated for N iterations, where N is the number of training steps:

1) Randomly choose inputs to present to the SOM;
2) On the basis of a Euclidean distance metric, find the output-layer node whose weights are most similar to the input;
3) Update the weight of that node and those of its neighbours according to the following equation:

$$w_{ji}(t) = w_{ji}(t-1) + \alpha(t-1)[ip_i(t-1) - w_{ji}(t-1)] \quad (1)$$

where $w_{ji}(t)$ is the weighting between node j and input i, ip_i is the i^{th} input, and α is the gain or learning rate (an empirically chosen adjustable parameter that can be adjusted to regulate the training speed);
4) Reduce neighbourhood size and learning rate as per the following two equations:

$$D = \lceil d_0(1 - t/N) \rceil \quad (2)$$

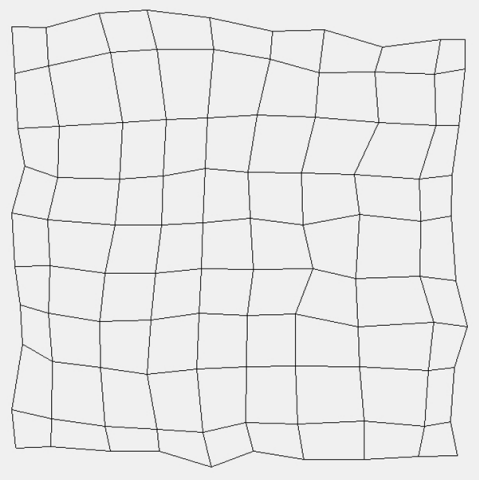

Figure 3. Network weights after training has been completed.

where d_0 is the initial neighbourhood size, t is the current updating/training iteration and N is the total number of iterations.

$$\alpha = \alpha_0(1 - t/N) \tag{3}$$

Typically the neighbourhood size begins large (e.g. one-half to one-third of the grid size). Several different forms of neighbourhood type can be used. In this paper, a simple square neighbourhood is used and neighbourhood size is restricted to integer values. After training has been completed, the weight values are once again plotted and shown in Figure 3.

B. Network Testing

Randomly chosen input patterns are applied and Euclidean distance competitions held to see which set of weights are most similar to the input patterns. Similar inputs pattern have been found to cause nodes that are adjacent in the output layer to win. This being the case, from Kohonen's definition [14], the neural network can be said to be organised: "The mapping is said to be ordered if the topological relations of the images and the patterns are similar". Using a skewed input distribution, where the second training input is chosen to be in the range [0,0.2] when the first training input is greater than 0.5, leads to the map shown in Figure 4.

This approach to testing and training, applied to the breast tumour RTS dataset, is discussed in Section V.

III. Tumour Shape and Electromagnetic Modeling

A. Tumour Shape Modelling

Shape and texture of the surface of a tumour are two of the most important characteristics used to differentiate between a benign and a malignant tumour. The tumour models used in this paper are based on the Gaussian Random Spheres (GRS) method [15], [16]. GRS can be modified mathematically to model both malignant and benign tumours of different sizes by varying the logarithmic radius and the mean radius α, respectively. The shape is determined by the radius vector, $\mathbf{r} = r(\theta, \psi)$, described in spherical coordinates (r, θ, ψ), by the logradius $s = s(\theta, \psi)$:

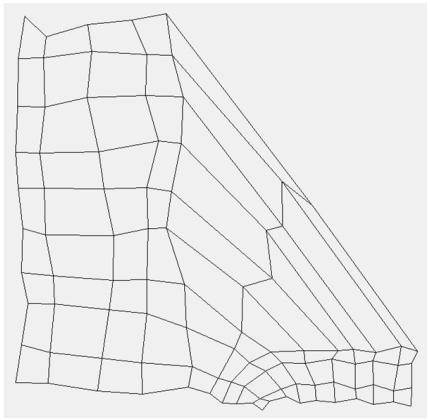

Figure 4. Plot of network weights for a skewed input distribution.

$$s(\theta, \psi) = \sum_{l=0}^{\infty} \sum_{m=-l}^{l} s_{lm} Y_{lm}(\theta, \psi) \tag{4}$$

$$r(\theta, \psi) = \alpha \exp\left[s(\theta, \psi) - \frac{1}{2}\beta^2\right] \tag{5}$$

In the equations above, β is the standard deviation of the logradius, s_{lm} are the spherical harmonic coefficients and Y_{lm} are the orthonormal spherical harmonics [15], [16]. Three different tumour models of one size are considered in this paper (macrolobulated benign, and 3 and 10-spiculed malignant tumours). Malignant tumours are represented by spiculed GRS, whereas benign tumours are modelled by macrolobulated GRS. Macrolobulated GRS are obtained by varying the correlation angle between 25 and 45 degrees and smooth GRS have a correlation angle between 50 and 90 degrees. Spiculed GRS are obtained by adding 3 or 10 spicules to smooth GRS. The average radius of all types of spheres are 2.5 mm. Ninety tumour models were developed (30 benign and 60 malignant of which 30 had three spicules and 30 had ten spicules), each having 4 recorded signals corresponding to 4 antennas.

In order to examine the effects of dielectric heterogeneity, a second set of models was created where fibroglandular tissue was introduced into the FDTD models. Fibroglandular tissue, extracted from the UWCEM Breast Phantom Repository [17], is introduced into the FDTD model (phantom ID 071904). A single piece of fibroglandular tissue is added to the FDTD models, as shown in Figure 5.

 ISBN: 978-1-61208-246-2

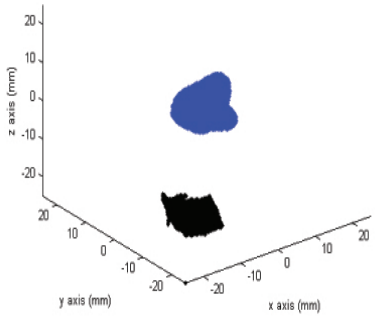

Figure 5. Example of the heterogeneous breast model. The tumour is shown in blue, while the fibroglandular tissue is shown in black.

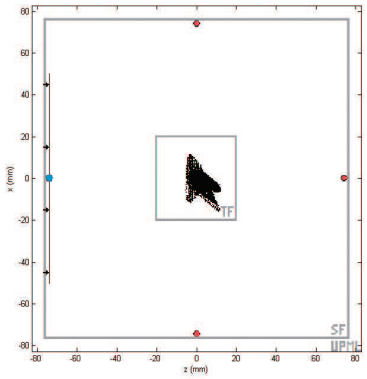

Figure 6. Cross-section of the 3D FDTD space lattice partitioned into Total Field (TF), Scattered Field (SF) and UPML regions, for a homogeneous breast model. The target, a spiculed tumour located at the centre of the TF in this example, is illuminated by a pulsed plane wave propagating in the +z direction (represented by a dark line) and backscatter is recorded at the first observer location: (0,0,-74) mm (represented by a blue circle). The remaining three antennas are represented by small red circles in the image.

B. Electromagnetic Modelling

The 90 tumours of size 2.5 mm are placed in a 3D Finite-Difference Time-Domain (FDTD) model. The FDTD model has a 0.5 mm cubic grid resolution and the backscattered signals were generated through a Total-Field/Scattered-Field (TF/SF) structure, in which the tumours and fibroglandular tissue are completely embedded in the Total Field (TF) [18], [19]. The TF/SF region has the following dimensions: the Scattered Field (SF) is a square prism with square bases measuring 153.5 mm on the side and height measuring 137.5 mm. The TF is located at the centre of the SF and is represented by a 50 mm-sided cube (the origin of the SF and the TF are at the point (0,0,0) mm). The dielectric properties of adipose, fibroglandular, and cancerous breast tissue are incorporated in the FDTD using a Debye formulation, based on the dielectric properties established by Lazebnik *et al.* [9], [10]. The TF/SF region is terminated with a 6 mm-layer Uni-axial Perfectly Matched Layer (UPML) which suppresses any boundary reflections [20].

A pulsed plane wave is transmitted towards the target from four different equidistant angles $(0°, 90°, 180°, 270°)$ and the resulting cross-polarised backscatter is recorded and analysed from antennas located at: (0,0,-74), (-74,0,0), (0,0,74) and (74,0,0) mm in (x,y,z) axes. The incident pulse is a modulated Gaussian pulse with center frequency at 6 GHz where the 1/e full temporal width of the Gaussian envelope is 160 picoseconds. For two transmitters, the pulse is linearly polarised in the x-y plane and transmitted in the z direction, and for the remaining transmitters, the pulse is polarised in the y-z plane and transmitted in the x direction. Each antenna is located in the SF at a distance of 74 mm from the center of the tumour, which is located at the centre of the TF. The acquired backscattered recorded signals are downsampled from 1200 GHz to 75GHz. Figure 6 shows a representation of the TF/SF grid, with the location of the origin of the first incident plane wave and respective observer point as well as the position of the tumour.

IV. Feature Extraction

The Discrete Wavelet Transform (DWT) is applied to the RTS and the resultant wavelet coefficients are obtained using low-pass decomposition filters. Subsequently, the low-pass band may be split again through further low-pass filters. In this paper, the chosen wavelet is *Coiflet 5* (established as the optimum wavelet by empirical analysis). The frequency band that is used for classification corresponds to the wavelet coefficients obtained from the low-pass band after a two-level decomposition, as these wavelet coefficients were found to give the best classification performance compared to other subbands, evaluated up to four levels of decomposition.

To identify the most relevant DWT coefficients for input to the SOM, a statistical analysis was performed on the dataset to identify the DWT components that exhibit the most statistically significant differences between malignant and benign tumours. A T-Test identifies the largest significant differences between the means of two independent sample groups, while taking the variances of both groups into account. The independent variable is whether the tumour is malignant or benign, while the dependent variable is the level of the DWT output. The 15 DWT components that exhibit the greatest differences between malignant and benign were identified, normalised, scaled to [-1,1] and employed for classification purposes

V. Results

Two distinct datasets were considered: data from simulations where the tumour is located in homogeneous breast tissue and a second set where fibroglandular tissue is present

 ISBN: 978-1-61208-246-2

(i.e., data from a more heterogeneous breast). Each of these datasets consisted of 360 tumour signals from models of size 2.5 mm each comprising of 15 normalised and scaled DWT values. In order to evaluate the classifier, each data-set is randomly shuffled and divided into ten combinations of 276 training and 84 testing tumours. The classification process is repeated 10 times for each of the ten files and the average performance of the classifier is calculated (note: all results presented is this paper are based on the performance of the test set).

For this particular study, weights were randomly initialized to be in the range [-1, 1] and training consisted of repeatedly applying scaled patterns of the 15 DWTs randomly chosen from the 276 tumour models in the training sample, until the network organised. The output layer consisted of a square 10x10 grid. The gain/learning rate (0.5), neighbourhood size (4) and number of training steps (5100) were empirically chosen. During training, the neural network had no input indicating whether the input pattern being presented to it belonged to a malignant or to a benign tumour model.

At the end of training, the network weights were frozen. At this point a Euclidean distance competition was held for each node in the output layer, for each of the 276 training tumour models in the training set. The tumour model pattern most similar to the weights of a node was then assigned to that node. Only at this point was the training data set examined to discover which inputs corresponded to malignant/benign tumour models.

Three-way classification is shown in the MammoMaps illustrated in Figure 7. Here, benign, 3-spiculed malignant and 10-spiculed malignant tumours are represented as green, orange and red regions, respectively.

In order to evaluate the performance of the three-way SOM classifier, the SOM is tested using a test sample of 84 tumours. Importantly, the DWT coefficients corresponding to these tumours have not previously been presented to the network. For testing, the 15 DWT values for each of the test tumour models are input to the trained network (whose weights are now frozen), a distance competition is held for each tumour model and a winning node found. The tumour is then classified based on which region it falls into on the SOM.

An average classification accuracy across 10 maps for each of the ten shuffled files was as follows:

- 99.5% for macrolobulated tumours
- 90.54% for 3 spiculed malignant tumours
- 88.28% for 10 spiculed malignant tumours

yielding an overall average accuracy of 92.77%.

The tumours fall into clear and distinct regions within the resultant SOM MammoMaps. Significantly, the region of benign tumours (shown in green) is separated in all cases from the highly malignant 10-spicule tumour region (shown in red) by the intermediate 3-spicule tumour region (shown in orange).

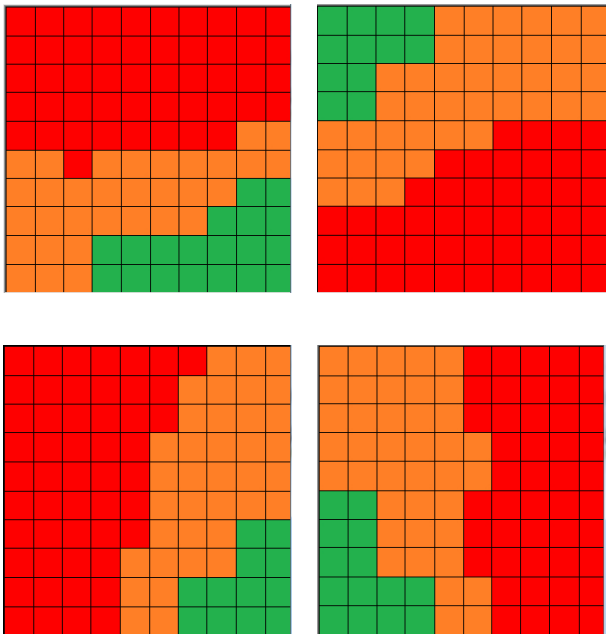

Figure 7. Four examples of three-way classification between benign macrolobulated (green), 3 spiculed malignant (orange) and 10 spiculed malignant (red) tumours using an SOM.

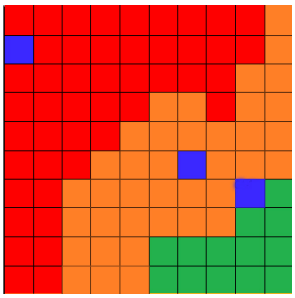

Figure 8. Tumour development tracking with an SOM. As the tumour (shown in blue) becomes increasingly malignant, it moves across the map from the green region to the red region.

Figure 8 shows a SOM being used to monitor a tumour (shown in blue) as it develops from benign macrolobulated to 3 spiculed malignant to 10 spiculed malignant. This highlights the significant potential of SOMs for tumour tracking, since SOMs preserve the input data topology.

VI. Conclusion and Future Work

In this study, "MammoMaps" have been shown to have the ability to differentiate between macrolobulated benign and two different levels of malignant tumours. Therefore, these "MammoMaps" have significant potential as a cancer classification or diagnosis tool.

 ISBN: 978-1-61208-246-2

However, more importantly they could also be used to monitor the development of a tumour due to the fact that "MammoMaps" preserve the topology of the input information. Therefore, a clinician could use these maps to determine whether a tumour is developing from benign to malignant (moving across the "MammoMap") or not (staying static on the "MammoMap"). Movement even within the benign region could indicate that the tumour is developing even before it is classified as malignant and so treatment could be offered to patients at a very early stage of their disease, when it is most effective. This potential will be further examined in future studies.

ACKNOWLEDGMENT

This research has been supported by Science Foundation Ireland (SFI) under the Starting Investigator Research Grant number 11/SIRG/12120, by Fundação para a Ciência e a Tecnologia under grant number SFRH/BPD/79735/2011 and by a Marie Curie Intra European Fellowship within the 7th European Community Framework Programme under REA grant agreement number 301269.

REFERENCES

[1] P. H. Huynh, A. M. Jarolimek, and S. Daye, "The false-negative mammogram," *RadioGraphics*, vol. 18, pp. 1137–1154, 1998.

[2] J. G. Elmore, M. B. Barton, V. M. Moceri, S. Polk, P. J. Arena, and S. W. Fletcher, "Ten-year risk of false positive screening mammograms and clinical breast examinations," *New Eng. J. Med.*, vol. 338, no. 16, pp. 1089–1096, 1998.

[3] F. M. Hall, J. M. Storella, D. Z. Silverstone, and G. Wyshak, "Non-palpaple breast-lesions, recommendations for biopsy based on suspicion of carcinoma at mammography," *Radiology*, vol. 167, no. 2, pp. 353–358, 1988.

[4] S. L. Nass, I. C. Henderson, and J. C. Lashof, *Mammography and Beyond: Developing Technologies for the early detection of breast cancer*. National Academy Press, 2001.

[5] S. S. Chaudhary, R. K. Mishra, A. Swarup, and J. M. Thomas, "Dielectric properties of normal and malignant human breast tissue at radiowave and microwave frequencies," *Indian J. Biochem. Biophys.*, vol. 21, pp. 76–79, 1984.

[6] A. J. Surowiec, S. S. Stuchly, J. R. Barr, and A. Swarup, "Dielectric properties of breast carcinoma and the surrounding tissues," *IEEE Trans. Biomed. Eng.*, vol. 35, no. 4, pp. 257–263, April, 1988.

[7] W. T. Joines, Y. Zhang, C. Li, and R. L. Jirtle, "The measured electrical properties of normal and malignant human tissues from 50 to 900 MHz," *Med. Phys*, vol. 21, no. 4, pp. 547–550, April, 1994.

[8] A. M. Campbell and D. V. Land, "Dielectric properties of female human breast tissue measured *in vitro* at 3.2 GHz," *Phys. Med. Biol.*, vol. 37, no. 1, pp. 193–210, 1992.

[9] M. Lazebnik, L. McCartney, D. Popovic, C. B. Watkins, M. J. Lindstrom, J. Harter, S. Sewall, A. Magliocco, J. H. Booske, M. Okoniewski, and S. C. Hagness, "A large-scale study of the ultrawideband microwave dielectric properties of normal breast tissue obtained from reduction surgeries," *Phys. Med. Biol.*, vol. 52, pp. 2637–2656, 2007.

[10] M. Lazebnik, D. Popovic, L. McCartney, C. B. Watkins, M. J. Lindstrom, J. Harter, S. Sewall, T. Ogilvie, A. Magliocco, T. M. Breslin, W. Temple, D. Mew, J. H. Booske, M. Okoniewski, and S. C. Hagness, "A large-scale study of the ultrawideband microwave dielectric properties of normal, benign and malignant breast tissues obtained from cancer surgeries," *Phys. Med. Biol.*, vol. 52, pp. 6093–6115, 2007.

[11] M. Nguyen and R. Rangayyan, "Shape analysis of breast masses in mammograms via the fractial dimension," in *Engineering in Medicine and Biology 27th Annual Conference*. IEEE, 2005, pp. 3210–3213.

[12] T. Kohonen, "The self-organizing map," *Proceedings of the IEEE*, vol. 78, no. 9, pp. 1464–1480, Sep. 1990.

[13] D. G. Roussinov and H. Chen, "A scalable self-organizing map algorithm for textual classification: A neural network approach to thesaurus generation," *Communication Cognition and Artificial Intelligence, Spring*, vol. 15, pp. 81–112, 1998.

[14] G. J. Deboeck and T. K. Kohonen, Eds., *Visual Explorations in Finance*, 1st ed. Secaucus, NJ, USA: Springer-Verlag New York, Inc., 1998.

[15] K. Muinonen, "Introducing the gaussian shape hypothesis for asteroids and comets," *Astronomy and Astrophysics*, vol. 332, pp. 1087–1098, 1998.

[16] ——, *Chapter 11: Light Scattering by Stochastically Shaped Particles*. Academic Press, 2000.

[17] E. Zastrow, S. K. Davis, M. Lazebnik, F. Kelcz, B. D. V. Veen, and S. C. Hagness. (2008) Database of 3d grid-based numerical breast phantoms for use in computational electromagnetics simulations. Online. Department of Electrical and Computer Engineering University of Wisconsin-Madison. [Online]. Available: http://uwcem.ece.wisc.edu/home.htm

[18] S. K. Davis, B. D. V. Veen, S. C. Hagness, and F. Kelcz, "Breast tumor characterization based on ultrawideband backscatter," *IEEE Trans. Biomed. Eng.*, vol. 55, no. 1, pp. 237–246, 2008.

[19] R. C. Conceicao, D. Byrne, M. O'Halloran, E. Jones, and M. Glavin, "Investigation of classifiers for early-stage breast cancer based on radar target signatures," *Progress in Electromagnetics Research*, vol. 105, pp. 295–311, 2010.

[20] A. Taflove and S. C. Hagness, *Computational Electrodynamics: The Finite-Difference Time-Domain Method*. Artech House Publishers, June, 2005.

 ISBN: 978-1-61208-246-2